Lifshitz Transitions Induced by Temperature and Surface Doping in Type-II Weyl Semimetal Candidate T_d-WTe$_2$

Qihang Zhang, Zhongkai Liu, Yan Sun, Haifeng Yang, Juan Jiang, Sung-Kwan Mo, Zahid Hussain, Xiaofeng Qian, Liang Fu, Shuhua Yao, Minghui Lu, Claudia Felser, Binghai Yan, Yulin Chen,* and Lexian Yang*

Using high resolution angle-resolved photoemission spectroscopy, we systematically investigate the electronic structure of T_d-WTe$_2$, which has attracted substantial research attention due to its diverse and fascinating properties, especially the predicted type-II topological Weyl semimetal (TWS) phase. The observed significant lattice contraction and the fact that our ARPES measurements are well reproduced by our ab initio calculations under reduced lattice constants support the theoretical prediction of a type-II TWS phase in T_d-WTe$_2$ at temperatures below 10 K. We also investigate the evolution of the electronic structure of T_d-WTe$_2$ and realize two-stage Lifshitz transitions induced by temperature regulation and surface modification, respectively. Our results not only shed light on the understanding of the electronic structure of T_d-WTe$_2$, but also provide a promising method to manipulate the electronic structures and physical properties of the type-II TWS T_d-XTe$_2$.

Topological Weyl semimetals (TWSs) are characterized by the existence of bulk Weyl fermions and topological surface Fermi-arcs connecting each pair of Weyl points (WPs) of opposite chirality.[1] Upon their discovery, TWSs have evoked enormous research interests due to their intriguing physical properties and broad application potential.[1–9] Soon after the establishment of the TWS phase in the transition metal mono-pnictide (TMMP) family,[10–17] the type-II TWS phase was theoretically proposed in T_d-XTe$_2$ (X = W, Mo) that violates the Lorentz symmetry,[18] thus the strongly tilted bulk Weyl cones introduce non-vanishing bulk (both electron and hole) Fermi pockets on the Fermi surface (FS).[18–35] Compared to the complicated distribution of 24 Weyl fermions in the TMMPs and their three-dimensional (3D) crystal structures,[10–15] T_d-XTe$_2$ not only has much more concise distribution of Weyl fermions, but also crystallizes into layered structure, thus providing a more promising material basis to design, process, and fabricate TWS-based electronic and spintronic devices.

Besides being recognized as type-II TWSs, T_d-XTe$_2$ materials are well known to possess other rich and intriguing physical properties, such as quantum spin Hall effect,[36–38] non-saturating magnetoresistance,[39,40] strong spin–orbit

Q. Zhang, Prof. Y. Chen, Prof. L. Yang
State Key Laboratory of Low Dimensional Quantum Physics
Department of Physics and Collaborative Innovation Center of Quantum Matter
Tsinghua University, Beijing 100084, P. R. China
E-mail: yulin.chen@physics.ox.ac.uk;
lxyang@tsinghua.edu.cn

Prof. Z. Liu, Dr. J. Jiang, Prof. Y. Chen
School of Physical Science and Technology
ShanghaiTech University
and CAS-Shanghai Science Research Center,
Shanghai 200031, P.R. China

Dr. Y. Sun, Prof. C. Felser, Prof. B. Yan
Max Planck Institute for Chemical Physics of Solids,
01187 Dresden, Germany

Dr. H. Yang, Dr. J. Jiang, Prof. Y. Chen
Department of Physics, Clarendon Laboratory
University of Oxford,
Parks Road, Oxford OX1 3PU, UK

(iD) The ORCID identification number(s) for the author(s) of this article can be found under https://doi.org/10.1002/pssr.201700209.

DOI: 10.1002/pssr.201700209

Dr. H. F. Yang
Laboratory of Functional Materials for Informatics
Shanghai Institute of Microsystem and Information Technology (SIMIT)
Chinese Academy of Sciences,
865 Changning Road, Shanghai 200050, P.R. China

Dr. J. Jiang, Dr. S.-K. Mo, Prof. Z. Hussain
Advanced Light Source
Lawrence Berkeley National Laboratory, Berkeley, CA 94720, USA

Dr. J. Jiang
Pohang Accelerator Laboratory
POSTECH, Pohang 790-784, Korea

Prof. X. Qian
Department of Materials Science and Engineering
College of Engineering and College of Science
Texas A&M University, College Station, TX 77843, USA

Prof. L. Fu
Department of Physics Massachusetts Institute of Technology,
Cambridge, MA 02139, USA

Prof. S. Yao, Prof. M. Lu
National Laboratory of Solid State Microstructures
Department of Materials Science and Engineering
Nanjing University, Nanjing 210093, P.R. China

coupling,[41] temperature-induced Lifshitz transition,[42] and pressure-enhanced superconductivity.[43,44] T_d-XTe_2 family of compounds thus serves as an ideal platform to investigate different emergent properties and their interplay in topological quantum materials. Despite tremendous efforts over the past couple of years,[21–35,40,41] however, the understanding of the detailed electronic structures of T_d-XTe_2 still remains elusive and controversial. For example, there exist controversies about the number of WPs and the assignment of the Fermi arcs[18–35]; a direct observation of the bulk Weyl fermions is still missing; and there is still an essential lack of systematic investigation of the evolution of their electronic structures with external parameters.

In this work, by performing systematic high-resolution angle-resolved photoemission spectroscopy (ARPES) measurements, we presented detailed electronic structure of T_d-WTe_2 and its evolution with temperature and surface modification. The measured band structure can be well reproduced by our ab initio calculations that predicted a type-II TWS phase under reduced lattice parameters. Consistently, we observed a significant lattice contraction at low temperatures, suggesting a temperature-induced topological phase transition from a normal metal to a type-II TWS in T_d-WTe_2. Moreover, we were able to realize two-stage Lifshitz transitions induced by temperature regulation and surface modification, respectively. Our work is not only instructive and incentive for the understanding of the type-II TWS phase in T_d-$WTe2$, but also establishes a feasible and controllable method to manipulate the fundamental electronic structures and physical properties of T_d-XTe_2.

Materials: High-quality single crystal T_d-WTe_2 was synthesized by the chemical vapor transport method with $TeBr_4$ as the transport additive. Polycrystalline WTe_2 was first obtained by solid reaction of high-purity (99.999%) W and Te powders in an evacuated quartz tube at $700\,^{\circ}C$ for 1 week. A total of 1 g polycrystalline WTe_2 and $TeBr_4$ ($3\,mg\,ml^{-1}$) were then mixed, thoroughly grounded, and sealed in an evacuated quartz tube which was heated in a two-zone furnace with a temperature gradient from 850 to $750\,^{\circ}C$ for another week. Then black shining pallets with typical size of $2 \times 1 \times 0.1\,mm^3$ were obtained. We have carefully calibrated our samples using temperature-dependent Raman and XRD measurements and confirmed the crystals are in the T_d-phase.[45]

ARPES: ARPES measurements were performed at beamline 10.0.1 of the Advanced Light Source (ALS) at Lawrence Berkeley National Laboratory, USA and beamline I05 of the Diamond Light Source (DLS), UK. The measurement pressure was kept below 3×10^{-11} torr at ALS and 9×10^{-11} torr at DLS, data were recorded by Scienta R4000 analyzers. The total convolved energy and angle resolutions were 16 meV and 0.2°, respectively. The fresh surface of T_d-WTe_2 for ARPES measurements was obtained by cleaving the high quality single crystal in situ along (001) cleavage plane. The surface dosing was conducted in situ by evaporating K atoms directly onto the cleaved sample surface at low temperature.

DFT Calculations: The electronic structure of T_d-WTe_2 was calculated by the density-functional theory (DFT) method implemented in the Vienna ab initio Simulation Package (VASP) using lattice constants $a = 3.456\,\mathring{A}$, $b = 6.213\,\mathring{A}$, and $c = 13.935\,\mathring{A}$ (less than the experimental lattice constants at 10 K). The exchange and correlation energy was considered in

the generalized gradient approximation (GGA) with Perdew–Burke–Ernzerhof (PBE)-based density function and the spin–orbit coupling (SOC) was included self-consistently. The energy cut off was set to 300 eV for the plane-wave basis. The tight binding matrix elements were calculated by projecting the Bloch wave functions to maximally localized Wannier functions (MLWFs).[46] The surface states were calculated from the half-infinite model using the interactive Green's function method.[47] K-doped sample surface was simulated in a slab model by putting a layer of K atoms on the top surface of T_d-WTe_2 and the thickness of the T_d-WTe_2 slab is 7 unit cells.

Overall Electronic Structure of T_d-WTe_2: The crystal structure of T_d-WTe_2 is shown in **Figure 1**(a). The lattice is strongly distorted, forming chains of W atoms along *b*-axis and canting Te-W octahedral. With decreasing temperature, the lattice shrinks along all three lattice axes with a volume expansion coefficient of about 7.2×10^{-5}/K from our temperature-dependent X-ray diffraction (XRD) measurements (Figure 1 (c)). The FS mapping over multiple Brillouin zones (BZs) in Figure 1(b) verifies the (001) cleavage and strongly anisotropic electronic structures of T_d-WTe_2 along k_x and k_y directions, which is consistent with its orthorhombic crystal structure in Figure 1(a).

According to our ab initio calculations, the type-II TWS phase in T_d-WTe_2 is extremely sensitive to the lattice parameters and only exists when the lattice constants are smaller than $a = 3.463\,\mathring{A}$, $b = 6.230\,\mathring{A}$, and $c = 14.000\,\mathring{A}$. Our temperature-dependent XRD measurements in Figure 1(c) suggest that T_d-WTe_2 indeed falls into the predicted type-II TWS phase, in consistence with previous report [18,48]. The shrinking lattice volume further suggests the possibility of a temperature-induced topological phase transition.[48] Using lattice constants $a = \mathring{A}$, $b = 6.213\,\mathring{A}$, and $c = 13.935\,\mathring{A}$ (less than the experimental values at 10 K), our ab initio calculations predicts four pairs of Weyl points in each BZ at $[(k_x, k_y, k_z), E] = [(\pm0.037, \pm0.220, 0)\,\mathring{A}^{-1}, E_F + 55\,meV]$ (W1) and $[(\pm0.056, \pm0.220, 0)\,\mathring{A}^{-1}, E_F + 70\,meV]$ (W2), respectively, as illustrated in Figure 1(d) and (e). Due to the strong tilting of the Weyl cones,[18] there exist both electron and hole pockets on the FS of T_d-WTe_2 (Figure 1(f)), which are connected by the surface Fermi arcs (highlighted by the green thick curve in the bottom panel of Figure 1(f)).

Figure 2(a) demonstrates a 3D intensity plot of the band structures of T_d-WTe_2 measured at 9 K, where we observe strongly anisotropic band structures along $\bar{\Gamma}$–$\bar{Y}$ and $\bar{\Gamma}$–$\bar{X}$. The fine structure of the FS consists of Fermi pockets located near $k_y = \pm0.2\,\mathring{A}^{-1}$ and $k_y = \pm0.4\,\mathring{A}^{-1}$ (Figure 2(b) (i), (ii)). The FS pockets are overall very small compared with the size of the BZ, suggesting low carrier density near E_F and the semimetal nature of T_d-WTe_2. The measured band structures along high-symmetry directions show general agreement with our ab initio calculations under reduced lattice parameters as compared in Figure 2 (c) ($\bar{Y}$–$\bar{\Gamma}$–$\bar{Y}$) and (e) ($\bar{X}$–$\bar{\Gamma}$–$\bar{X}$). We note that the predicted trivial surface state (marked as SS in Figure 2(c)(ii)) is absent in our measurement, suggesting that the cleavage surface is type A as reported in Ref. [27]. From the peaks in the momentum distribution curve (MDC) at E_F (Figure 2(d)), we can resolve the Fermi crossings of the bands contributing to the FS. Clearly, the two Fermi pockets near $\pm0.4\,\mathring{A}^{-1}$ are electron pockets (e1) while the other four are
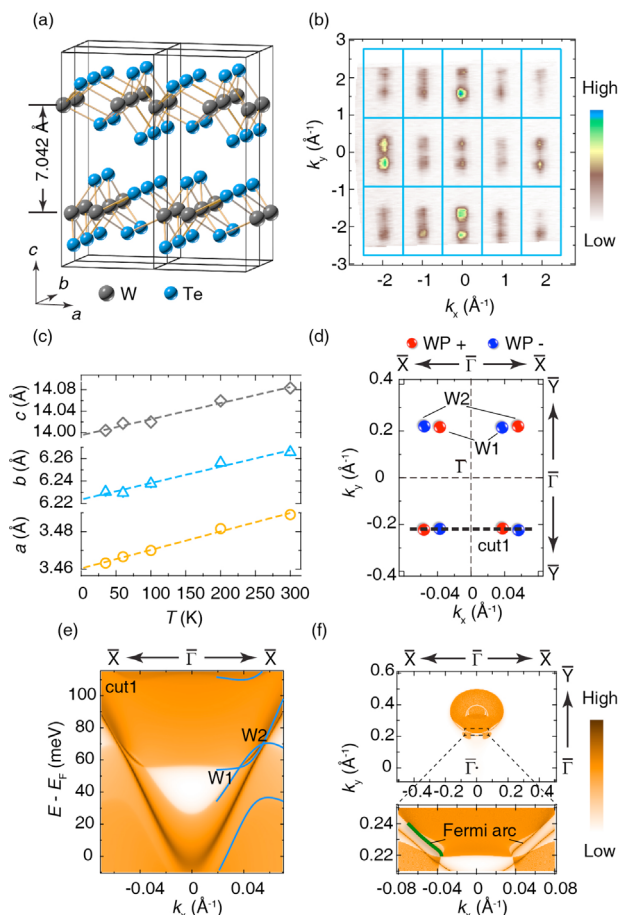
Figure 1. Basic characterization of T_d-WTe$_2$. a) The crystal structure of T_d-WTe$_2$ at room temperature. The W atoms form zigzag chains in the b-direction and the flat Te layers wrinkle to compensate the lattice distortion. b) Measured Fermi surface (FS) in multiple Brillouin zones (BZs). The blue rectangles indicate the surface BZs. c) The lattice constants of T_d-WTe$_2$ measured by X-ray diffraction as a function of temperature. d) The predicted locations of Weyl points (WPs) in the projected surface BZ. The WPs with different chirality are indicated by red and blue dots, respectively. e) The calculated spectral function of T_d-WTe$_2$ near Weyl points along cut #1 as marked in panel (d). The solid blue curves are the calculated bulk bands. f) Top: calculated constant energy contour of T_d-WTe$_2$ at 55 meV above the Fermi energy (E_F). Bottom: the zoom-in plot of the rectangular in top panel showing surface Fermi arcs (green curve) connecting the electron and hole pockets. The ab initio claculations were conducted with lattice parameters $a = 3.456$ Å, $b = 6.213$ Å, and $c = 13.935$ Å (less than lattice constants at 10 K).

hole pockets (h1 and h2). The band structures along cuts #3 and #4 confirm that there are two hole-like bands and one-electron like band crossing E_F in each half of the BZ (Figure 2(f) and (g)). The different numbers of Fermi pockets in our work and previous reports may be due to different experimental conditions and sample quality.[27,28,41,42] For example, in Ref. [27], Bruno et al. observed spin split Fermi pockets and obtained twice the number of Fermi pockets as in our work.

Apparently, the measured hole pockets are almost twice the size of electron pockets, excluding a simple carrier compensation on the $\bar{\Gamma}$–$\bar{X}$–$\bar{Y}$ plane. Yet, a perfect carrier compensation may still be established if the k_z dispersion of the energy bands is taken into account, which will play a decisive role in the non-saturating magnetoresistance in T_d-WTe$_2$.[34,39,40]

Two-Stage Lifshitz Transition Induced by Temperature: **Figure 3** shows the evolution of the FS topology and electronic structure with temperature. At 9 K, we observe two hole pockets and one electron pocket in each half of the BZ (Figure 3(a)(i)). With increasing temperature, we observe clear change in the size and topology of Fermi pockets. The electron pockets at $k_y = \pm 0.4$ Å^{-1} enlarge while the hole pockets at $k_y = \pm 0.2$ Å^{-1} shrink and become blurred, which indicates an upward shift of E_F (Figure 3(a) (i)–(vi)), in consistence with previous report.[42] Near 90 K, the smaller hole pocket h1 disappears on the FS, suggesting a temperature-induced change of the FS topology or a Lifshitz transition. With temperature further increasing, h2 also disappears at 220 K and leaves a single pair of electron pockets on the FS, suggesting a two-stage Lifshitz transition, i.e., the FS topology changes twice subsequently with increasing temperature.

Consistently, we observe a systematic shift of energy bands at high binding energies as shown in Figure 3(b) (i)–(vi), which can be tracked by the peaks in the energy distribution curves at the $\bar{\Gamma}$ point (Figure 3(c)). With increasing temperature, the bands gradually shift toward high binding energies. By tracking the bottom of the electron band and the EDC peaks at the $\bar{\Gamma}$ point, we observe a nearly rigid shift of the bands for about 30 meV from 9 to 200 K. Yet, we also notice some non-rigid band shift. For example, the Γ_2 and Γ_3 bands approach each other at high temperatures. The band-top of the Γ_3 and Γ_2 bands sink below E_F near 90 K (Figure 3(b) (iv)) and 220 K (Figure 3(b) (vi)), respectively, supporting the subsequent disappearance of h1 and h2 pockets on the FS and temperature-induced Lifshitz transitions in T_d-WTe$_2$.[42] The drastic variation of the size and topology of Fermi pockets may break the delicate carrier compensation and reduce the magnetoresistance of T_d-WTe$_2$ at high temperature.[40]

Surface-Modification Induced Lifshitz Transition: Since the surface electronic structures of T_d-WTe$_2$ strongly depend on the surface condition and the WPs reside above E_F of the pristine crystal (Figure 1(e)), we investigate the evolution of the electronic structures of T_d-WTe$_2$ with the surface modification by systematic in situ K dosing in **Figure 4**. The absorption of K atoms is monitored by the characteristic K 3p peak in the core level photoemission spectra (Figure 4(a)). We address that the change of electronic structure occur only and immediately after surface K-doping is initiated, excluding significant contamination effect from other residual gases. With increasing K dosing time, the electron (hole) pockets on the FS enlarge (shrink) as shown in Figure 4(b). Consistently, the band dispersions along $\bar{Y}$–$\bar{\Gamma}$–$\bar{Y}$ shift toward high binding energies gradually. Resembling the evolution of the band structure with temperature, the top of the Γ_3 and Γ_2 bands subsequently sink below E_F after K dosing for 810 and 2190 s, respectively, suggesting a two-stage Lifshitz transition induced by surface modification (Figure 4(b) and (c)). As summarized in Figure 4(d), E_F can be tuned upward for as large as 90 meV, allowing the approaching to both W1 and W2 in T_d-WTe$_2$. Unfortunately, the length of the predicted Fermi arc is too short (less than 1% of the BZ) to be resolved in our experiment.
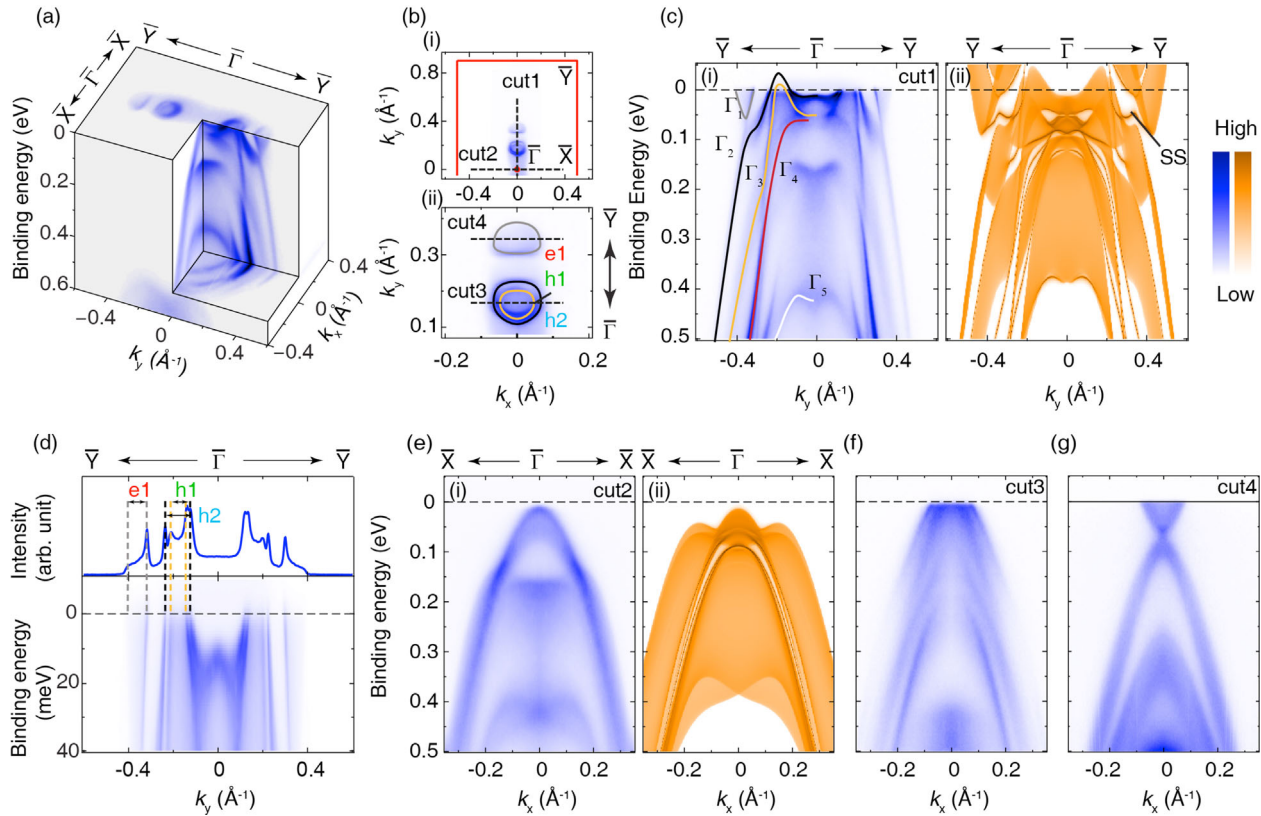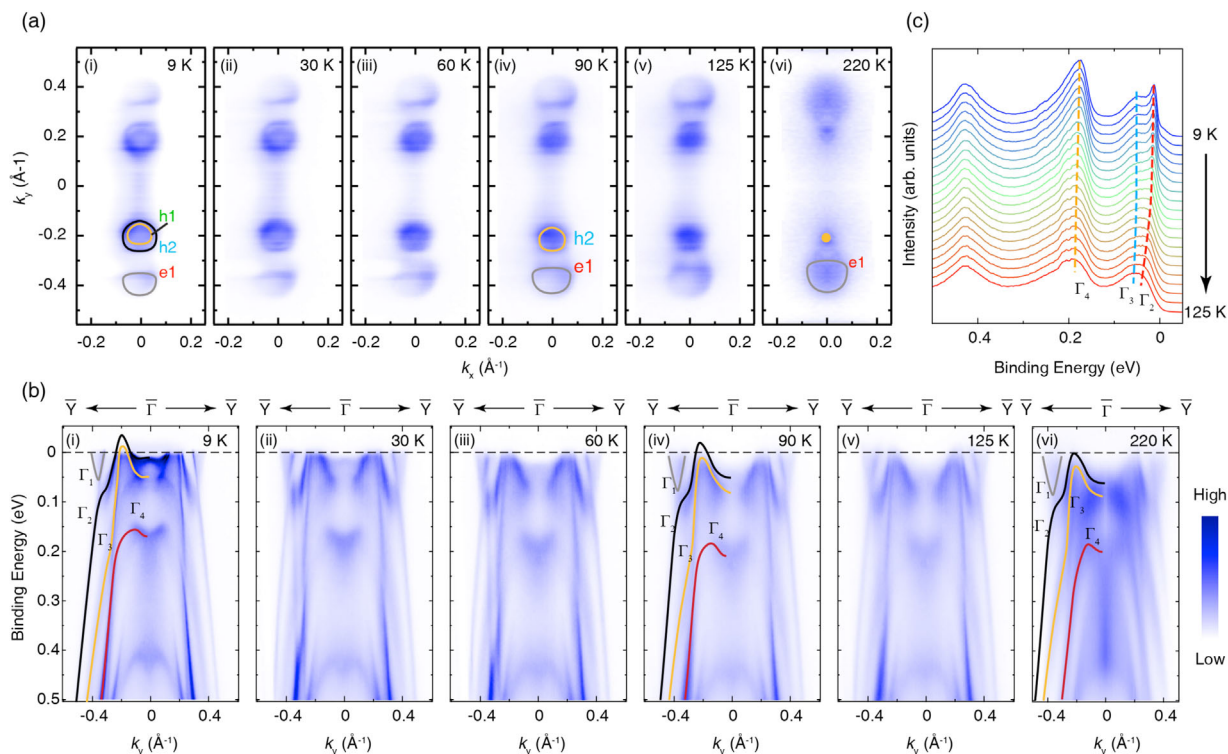
Figure 2. Band structure along high symmetric directions and Fermi surface (FS) map at 9 K. a) 3D illustration of the band structure of T_d-WTe$_2$. b) (i) Fermi surface map in the first BZ. The red lines indicate the surface BZ. (ii) The zoom-in plot of the FS. The colored curves are the guides to the eyes for the Fermi pockets. The black-dashed lines mark different measurement cuts. c) The comparison of the measured (i) and calculated (ii) band structure along the $\bar{Y}$–$\bar{\Gamma}$–$\bar{Y}$ direction. The solid curves are the guides to the eyes for the band dispersions. d) The zoom-in plot of the dispersion near the E_F showing the Fermi crossings of the hole and electron pockets together with the momentum distribution curve at E_F. e) The comparison of the measured (i) and calculated (ii) band structure along the $\bar{X}$–$\bar{\Gamma}$–$\bar{X}$ direction. f and g) Band structures along cuts #3 and #4 as marked in panel (b).

Interestingly, after significant K dosing on the surface, the band structure shows a dramatic change, which is dominated by two cross-shape features near 200 and 500 meV below E_F, respectively (Figure 4(e)). Our ab initio calculation well reproduces these X-shape features by modeling the system with T_d-WTe$_2$ covered by a layer of K atoms as shown in Figure 4 (f), which further supports that our observation is due to surface K-doping instead of surface contamination. After K doping, the bulk bands of T_d-WTe$_2$ shifts toward high binding energies and the spectral weight around the $\bar{\Gamma}$ point is dominated by additional bands from the hybridized states at the surface region, in consistence with our experiment (Figure 4 (e)). Although the bulk band dispersions of T_d-WTe$_2$ was not changed too much, the induced Lifshitz transition and the emergence of additional state from the hybridization between T_d-WTe$_2$ and K layer suggest a possible change of the physical properties of the system, such as extremely large magnetoresistance, superconductivity, etc.

Discussion: T_d-WTe$_2$ and T_d-MoTe$_2$ share common properties and electronic structures. While the type-II TWS phase has been experimentally verified in T_d-MoTe$_2$,[22–26,29] a direct

observation of the non-trivial surface Fermi arc in T_d-WTe$_2$ is still under debate due to the extremely short Fermi arc (comparable with the momentum resolution) and overlapped bulk Fermi pockets. We emphasize that our measured band structure can be better reproduced by our ab initio calculations under reduced lattice parameter, which supports a type-II TWS phase in T_d-WTe$_2$. Yet, in order to provide unambiguous evidence for the type-II TWS phase, it is important to lengthen the Fermi arc. It is well-known that the Fermi arc in T_d-WTe$_2$ can be extended by Mo doping.[20] The observed lattice contraction at low temperature (Figure 1(c)) together with our ab initio calculation provides another way to substantially lengthen the Fermi arc, which is instructive and incentive for the design and manipulation of the type-II TWS phase in T_d-WTe$_2$ via, e.g., temperature regulation and/or application of strain by fabricating ultra-thin films of T_d-WTe$_2$ on proper substrates.

The established two-stage Lifshitz transitions induced by temperature regulation and surface modification also provide a feasible method to manipulate the electronic structure of T_d-WTe$_2$. While the surface doping induced Lifshitz transition

ADVANCED
SCIENCE NEWS

www.advancedsciencenews.com

physica
status
solidi **rrl**

www.pss-rapid.com

Figure 3. Evolution of the band structures of T_d-WTe$_2$ with temperature. a) The evolution of the Fermi surface with temperature. b) The evolution of the band structure along the $\bar{Y}$–$\bar{\Gamma}$–$\bar{Y}$ direction with increasing temperature. c) The evolution of the energy distribution curve (EDC) near the $\bar{\Gamma}$ point with increasing temperature. The colored-dashed curves are the guides to the eyes for the shift of the bands.

is simply due to the charge doping effect, the mechanism for the temperature-induced Lifshitz transition or substantial E_F shift in a metallic system T_d-WTe$_2$ is still intricate. We argue that both the unique electronic structure and lattice thermal expansion should play important roles. From electronic structure perspective, the small and possibly compensated FS pockets of T_d-WTe$_2$ provide an essential prerequisite for the tunability of the Fermi level.[42] From the lattice perspective, the large lattice expansion coefficient (Figure 1(c)) and the sensitivity of the band structure to the lattice parameters will provoke a drastic band reconstruction with temperature. Especially, the hole like bands form a saddle point near the $\bar{\Gamma}$ point (Figure 2(c) and (e)), which results in a large density of states (DOS) near E_F. With increasing temperature, the lattice expansion will dramatically change the DOS near E_F (Figure 3 (b)), which itself has to adjust in order to keep the charge neutrality, inducing a significant Fermi level shift. Besides the unique electronic structure and large lattice expansion, other effects such as charge localization or delocalization and similar temperature effects in degenerate semiconductor as proposed to explain the temperature-induced Lifshitz transition in (Zr, Hf)Te$_5$ cannot be fully excluded from the mechanism of temperature-induced Lifshitz transition in T_d-WTe$_2$.[49,50] We note that a recent DFT calculation fails in reproducing the observed band evolution,[51] possibly because it used a much smaller volume expansion coefficient obtained

from calculation (about 1.7×10^{-5}/K compared with 7.2×10^{-5}/K from our experiment).

Finally, we observe a dramatic change of the electronic structure of T_d-WTe$_2$ after surface doping with K atoms. Although the K-doping induced Lifshitz transition is within expectation, the observed non-rigid shift of energy bands (Figure 4(d) and (e)) and X-shaped bands alludes more complex variation of the system with surface modification. We speculate that the enhanced surface potential gradient barrier should play an important role. Regarding the topological nature of the system, although the bulk topology will not be changed by simple surface doping, the connection topology of the surface Fermi arcs may be affected by surface modification.[52] Moreover, the K atoms may intercalate into the crystal considering the large interlayer distance in T_d-WTe$_2$, which will affect the interlayer coupling and change the bulk band structure. Further experimental and theoretical efforts are strongly required to fully understand the band evolution and the effect of K dosing on physical properties and type-II TWS phase in T_d-WTe$_2$.

In summary, we present a systematic study of the electronic structure of T_d-WTe$_2$. The observed significant lattice contraction at low temperatures provides a structural basis for the predicted type-II TWS phase. In addition, we realize two-stage Lifshitz transitions with temperature regulation and surface modification, respectively. These findings will shed
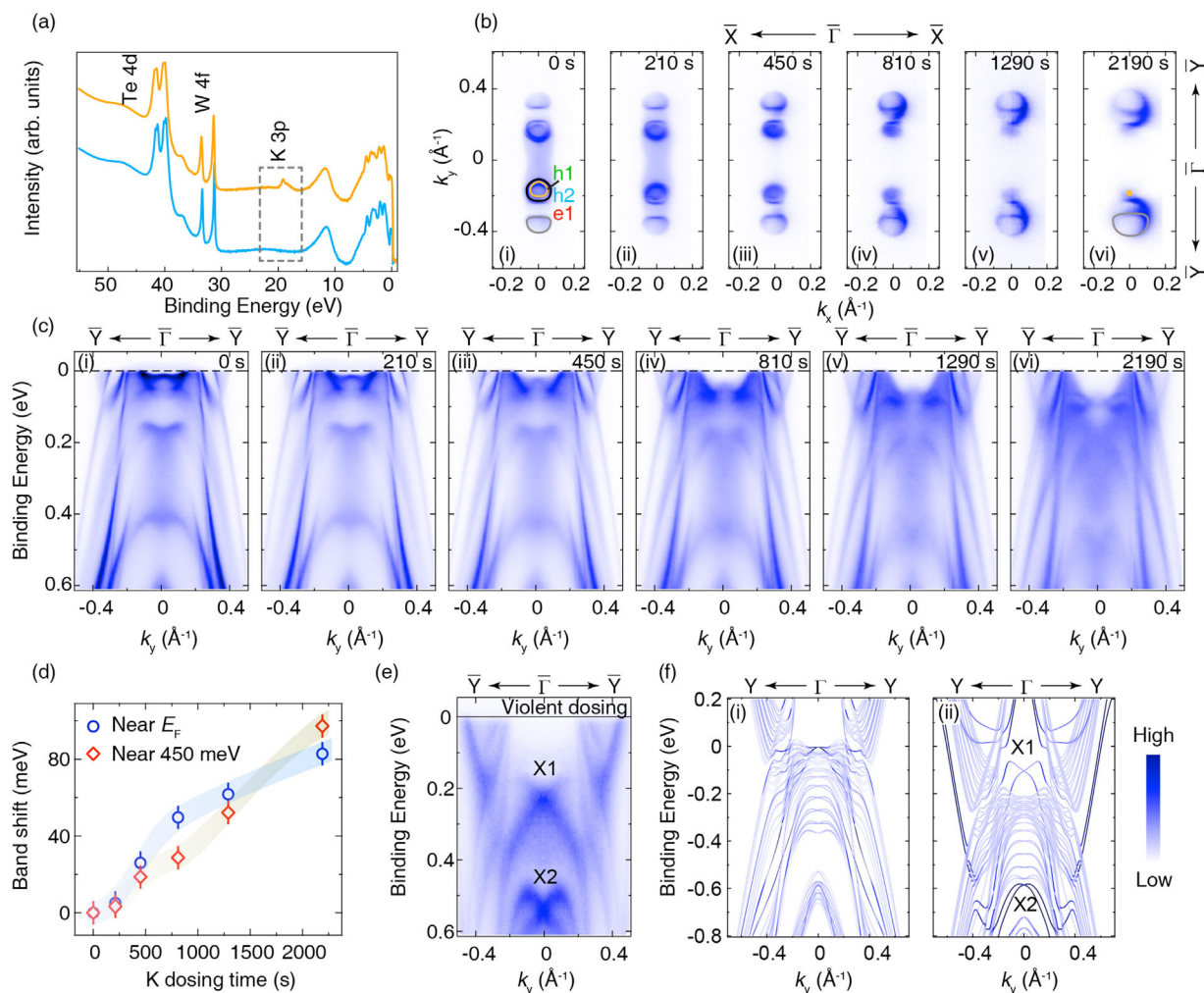
Figure 4. Band evolution with surface modification. a) The photoemission core level spectra with characteristic W, Te, and K peaks before (blue) and after (orange) potassium dosing. b) The evolution of the FS of WTe_2 with potassium dosing. c) The evolution of the band structure along the $\bar{Y}-\bar{\Gamma}-\bar{Y}$ direction with K dosing. d) The summarized band shift as a function of surface dosing time. The red diamond and blue circles are obtained by tracking the bands at different binding energies. e) The band structure of K-dosed WTe_2 after significant surface dosing. Two prominent X-shape features (X1 and X2) were observed. f) The calculated band structure on the (i) pristine and (ii) K-dosed surfaces. X1 and X2 were well reproduced by the theoretical calculation.

light on the understanding of the rich and unusual properties of T_d-WTe_2.

Acknowledgments

Conflict of Interest

The authors declare no conflict of interest.

Keywords

[1] X. Wan, A. M. Turner, A. Vishwanath, S. Y. Savrasov, *Phys. Rev. B* **2011**, *83*, 205101.

[2] A. A. Burkov, L. Balents, *Phys. Rev. Lett.* **2011**, *107*, 127205.

[3] B. Singh, A. Sharma, H. Lin, M. Z. Hasan, R. Prasad, A. Bansil, *Phys. Rev. B* **2012**, *86*, 115208.

[4] G. Xu, H. -M. Weng, Z. -J. Wang, X. Dai, Z. Fang, *Phys. Rev. Lett.* **2011**, *107*, 186806.

[5] M. Hirayama, R. Okugawa, S. Ishibashi, S. Murakami, T. Miyake, *Phys. Rev. Lett.* **2015**, *114*, 206401.

[6] J. Liu, D. Vanderbilt, *Phys. Rev. B* **2014**, *90*, 155316.

[7] P. Hosur, *Phys. Rev. B* **2012**, *86*, 195102.

[8] P. E. C. Ashby, J. P. Carbotte, *Phys. Rev. B* **2013**, *87*, 245131.

[9] K. Landsteiner, *Phys. Rev. B* **2014**, *89*, 075124.

[10] H. Weng, C. Fang, Z. Fang, B. A. Bernevig, X. Dai, *Phys. Rev. X* **2015**, *5*, 011029.

[11] S. -M. Huang, S. -Y. Xu, I. Belopolski, C. -C Lee, G. -Q. Chang, B. -K. Wang, N. Alidoust, G. Bian, M. Neupane, C. -L. Zhang, S. Jia, A. Bansil, H. Lin, M. Z. Hasan, *Nature Commun.* **2015**, *6*, 7373.

[12] S. -Y. Xu, N. Alidoust, I. Belopolski, Z. Yuan, G. Bian, T. -R. Chang, H. Zheng, V .N. Strocov, D. S. Sanchez, G. Chang, C. Zhang, D. Mou, Y. Wu, L. Huang, C. -C. Lee, S. -M. Huang, B. Wang, A. Bansil, H. -T. Jeng, T. Neupert, A. Kaminski, H. Lin, S. Jia, M. Zahid Hasan, *Nature Phys.* **2015**, *11*, 748.

[13] B. Q. Lv, H. M. Weng, B. B. Fu, X. P. Wang, H. Miao, J. Ma, P. Richard, X. C. Huang, L. X. Zhao, G. F. Chen, Z. Fang, X. Dai, T. Qian, H. Ding, *Phys. Rev. X* **2015**, *5*, 031013.

[14] L. X. Yang, Z. K. Liu, Y. Sun, H. Peng, H. F. Yang, T. Zhang, B. Zhou, Y. Zhang, Y. F. Guo, M. Rahn, D. Prabhakaran, Z. Hussain, S. K. Mo, C. Felser, B. Yan, Y. L. Chen, *Nature Phys.* **2015**, *11*, 728.

[15] Z. K. Liu, L. X. Yang, Y. Sun, T. Zhang, H. Peng, H. F. Yang, C. Chen, Y. Zhang, Y. F. Guo, D. Prabhakaran, M. Schmidt, Z. Hussain, S. K. Mo, C. Felser, B. Yan, Y. L. Chen, *Nature Mater.* **2016**, *15*, 27.

[16] B. Q. Lv, N. Xu, H. M. Weng, J. Z. Ma, P. Richard, X. C. Huang, L. X. Zhao, G. F. Chen, C. E. Matt, F. Bisti, V. N. Strocov, J. Mesot, Z. Fang, X. Dai, T. Qian, M. Shi, H. Ding, *Nature Phys.* **2015**, *11*, 724.

[17] S. -Y. Xu, I. Belopolski, N. Alidoust, M. Neupane, G. Bian, C. L. Zhang, R. Sankar, G. Q. Chang, Z. J. Yuan, C. -C. Lee, S. -M. Huang, H. Zheng, J. Ma, S. Daniel Sanchez, B. K. Wang, A. Bansil, F. C. Chou, P. Pavel Shibayev, H. Lin, S. Jia, M. Zahid Hasan, *Science* **2015**, *349*, 613.

[18] A.A. Soluyanov, D. Gresch, Z. Wang, Q. Wu, M. Troyer, X. Dai, B. A. Bernevig, *Nature* **2015**, *527*, 495.

[19] Y. Sun, Y. Sun, S. -C. Wu, M. N. Ali, C. Felser, B. Yan, *Phys. Rev. B* **2015**, *92*, 161107.

[20] T. -R. Chang, S. -Y. Xu, G. Chang, C. -C. Lee, S. -M. Huang, B. Wang, G. Bian, H. Zheng, D. S. Sanchez, I. Belopolski, N. Alidoust, M. Neupane, A. Bansil, H. -T. Jeng, H. Lin, M. Zahid Hasan, *Nature Commun.* **2016**, *7*, 10639.

[21] K. Deng, G. L. Wan, P. Deng, K. N. Zhang, S. J. Ding, E. Wang, M. Z. Yan, H. Q. Huang, H. Y. Zhang, Z. L. Xu, J. Denlinger, A. Fedorov, H. T. Yang, W. H. Duan, H. Yao, Y. Wu, S. S. Fan, H. J. Zhang, X. Chen, S. Y. Zhou, *Nature Phys.* **2016**, *12*, 1105.

[22] J. Jiang, Z. K. Liu, Y. Sun, H. F. Yang, C. R. Rajamathi, Y. P. Qi, L. X. Yang, C. Chen, H. Peng, C. C. Hwang, S. Z. Sun, S. K. Mo, I. Vobornik, J. Fujii, S. S. Parkin, C. Felser, B. H. Yan, Y. L. Chen, *Nature Commun.* **2017**, *8*, 13973.

[23] A. J. L. Huang, S. Nie, Y. Ding, Q. Gao, C. Hu, S. He, Y. Zhang, C. Wang, B. Shen, J. Liu, P. Ai, L. Yu, X. Sun, W. Zhao, S. Lv, D. Liu, C. Li, Y. Zhang, Y. Hu, Y. Xu, L. Zhao, G. Liu, Z. Mao, X. Jia, F. Zhang, S. Zhang, F. Yang, Z. Wang, Q. Peng, H. Weng, X. Dai, Z. Fang, Z. Xu, C. Chen, X.J. Zhou **2016**, arXiv:1604.01706.

[24] N. Xu, Z. J. Wang, A. P. Weber, A. Magrez, P. Bugnon, H. Berger, C. E. Matt, J. Z. Ma, B. B. Fu, B. Q. Lv, N. C. Plumb, M. Radovic, E. Pomjakushina, K. Conder, T. Qian, J. H. Dil, J. Mesot, H. Ding, M. Shi, **2016**, arXiv:1604.02116.

[25] Z. Wang, D. Gresch, A. A. Soluyanov, W. Xie, S. Kushwaha, X. Dai, M. Troyer, R. J. Cava, B. A. Bernevig, *Phys. Rev. Lett.* **2016**, *117*, 056805.

[26] L. Huang, T. M. McCormick, M. Ochi, Z. Zhao, M. T. Suzuki, R. Arita, Y. Wu, D. Mou, H. Cao, J. Yan, N. Trivedi, A. Kaminski, *Nature Mater.* **2016**, *15*, 1155.

[27] F. Y. Bruno, A. Tamai, Q. S. Wu, I. Cucchi, C. Barreteau, A. de la Torre, S. McKeown Walker, S. Riccò, Z. Wang, T. K. Kim, M. Hoesch, M. Shi, N. C. Plumb, E. Giannini, A. A. Soluyanov, F. Baumberger, *Phys. Rev. B* **2016**, *94*, 121112.

[28] C. Wang, Y. Zhang, J. Huang, S. Nie, G. Liu, A. Liang, Y. Zhang, B. Shen, J. Liu, C. Hu, Y. Ding, D. Liu, Y. Hu, S. He, L. Zhao, L. Yu, J. Hu, J. Wei, Z. Mao, Y. Shi, X. Jia, F. Zhang, S. Zhang, F. Yang, Z. Wang, Q. Peng, H. Weng, X. Dai, Z. Fang, Z. Xu, C. Chen, X. J. Zhou, *Phys. Rev. B* **2016**, *94*, 241119.

[29] A. Tamai, Q. S. Wu, I. Cucchi, F. Y. Bruno, S. Riccò, T. K. Kim, M. Hoesch, C. Barreteau, E. Giannini, C. Besnard, A. A. Soluyanov, F. Baumberger, *Phys. Rev. X* **2016**, *6*, 031021.

[30] J. Sánchez-Barriga, M. G. Vergniory, D. Evtushinsky, I. Aguilera, A. Varykhalov, S. Blügel, O. Rader, *Phys. Rev. B* **2016**, *94*, 161401.

[31] Y. Wu, D. Mou, N. H. Jo, K. Sun, L. Huang, S.L. Bud'ko, P. C. Canfield, A. Kaminski, *Phys. Rev. B* **2016**, *94*, 121113.

[32] B. Feng, Y. -H. Chan, Y. Feng, R. -Y. Liu, M. -Y. Chou, K. Kuroda, K. Yaji, A. Harasawa, P. Moras, A. Barinov, W. Malaeb, C. Bareille, T. Kondo, S. Shin, F. Komori, T. -C. Chiang, Y. Shi, I. Matsuda, *Phys. Rev. B* **2016**, *94*, 195134.

[33] M. Sakano, M. S. Bahramy, H. Tsuji, I. Araya, K. Ikeura, H. Sakai, S. Ishiwata, K. Yaji, K. Kuroda, A. Harasawa, S. Shin, K. Ishizaka, **2017**, *95*, 121101.

[34] Y. Wu, N. H. Jo, D. Mou, L. Huang, S. L. Bud'ko, P. C. Canfield, A. Kaminski, *Phys. Rev. B* **2017**, *95*, 195138.

[35] P. K. Das, D. Di Sante, I. Vobornik, J. Fujii, T. Okuda, E. Bruyer, A. Gyenis, B.E. Feldman, J. Tao, R. Ciancio, G. Rossi, M. N. Ali, S. Picozzi, A. Yadzani, G. Panaccione, R.J. Cava, *Nature Commun.* **2016**, *7*, 10847.

[36] X. Qian, J. Liu, L. Fu, J. Li, *Science* **2014**, *346*, 1344.

[37] Z. Y. Fei, T. Palomaki, S. Wu, W. Zhao, X. Cai, B. Sun, P. Nguyen, J. Finney, X. D. Xu, D. H. Cobden, *Nature Phys.* **2017**, *13*, 677.

[38] S. Tang, C. Zhang, D. Wong, Z. Pedramrazi, H. -Z. Tsai, C. Jia, B. Moritz, M. Claassen, H. Ryu, S. Kahn, J. Jiang, H. Yan, M. Hashimoto, D. Lu, R. G. Moore, C. -C. Hwang, C. Hwang, Z. Hussain, Y. Chen, M. M. Ugeda, Z. Liu, X. Xie, T. P. Devereaux, M. F. Crommie, S. -K. Mo, Z. -X. Shen, *Nature Phys.* **2017**, *13*, 683.

[39] M. N. Ali, J. Xiong, S. Flynn, J. Tao, Q. D. Gibson, L. M. Schoop, T. Liang, N. Haldolaarachchige, M. Hirschberger, N. P. Ong, R. J. Cava, *Nature* **2014**, *514*, 205.

[40] I. Pletikosić, M. N. Ali, A. V. Fedorov, R. J. Cava, T. Valla, *Phys. Rev. Lett.* **2014**, *113*, 216601.

[41] J. Jiang, F. Tang, X. C. Pan, H. M. Liu, X. H. Niu, Y. X. Wang, D. F. Xu, H. F. Yang, B. P. Xie, F. Q. Song, P. Dudin, T. K. Kim, M. Hoesch, P. K. Das, I. Vobornik, X. G. Wan, D. L. Feng, *Phys. Rev. Lett.* **2015**, *115*, 166601.

[42] Y. Wu, N. H. Jo, M. Ochi, L. Huang, D. Mou, S. L. Bud'ko, P. C. Canfield, N. Trivedi, R. Arita, A. Kaminski, *Phys. Rev. Lett.* **2015**, *115*, 166602.

[43] X. -C. Pan, X. Chen, H. Liu, Y. Feng, Z. Wei, Y. Zhou, Z. Chi, L. Pi, F. Yen, F. Song, X. Wan, Z. Yang, B. Wang, G. Wang, Y. Zhang, *Nature Commun.* **2015**, *6*, 7805.

[44] Y. -P. Qi, P. G. Naumov, M. N. Ali, C. R. Rajamathi, W. Schnelle, O. Barkalov, M. Hanfland, S. -C. Wu, C. Shekhar, Y. Sun, Vicky Süß, M. Schmidt, U. Schwarz, E. Pippel, P. Werner, R. Hillebrand, T. Förster, E. Kampert, S. Parkin, R. J. Cava, C. Felser, B. H. Yan, S. A. Medvedev, *Nature Commun.* **2016**, *7*, 11038.

[45] Y.-Y. Lv, L. Cao, X. Li, B.-B. Zhang, K. Wang, B. Pang, L. G. Ma, D. J. Lin, S.-H. Yao, J. Zhou, Y. B. Chen, S. T. Dong, W. C. Liu, M.-H. Lu, Y. L. Chen, Y.-F. Chen, *Sci. Rep.* **2017**, *7*, 44587.

[46] J. R. Y. A. A. Mostofi, Y. -S. Lee, I. Souza, D. Vanderbilt, N. Marzari, *Comput. Phys. Commun.* **2008**, *178*, 685.

[47] J. M. L. S. M. P. Lopez Sancho, J. Rubio, *J. Phys. F: Met. Phys.* **1984**, *14*, 1205.

[48] Y. -Y. Lv, X. Li, B. -B. Zhang, W. Y. Deng, S. -H. Yao, Y. B. Chen, J. Zhou, S. -T. Zhang, M. -H. Lu, L. Zhang, M. Tian, L. Sheng, Y. -F. Chen, *Phys. Rev. Lett.* **2017**, *118*, 096603.

[49] Y. Zhang, et al., *Nature Commun.* **2017**, *8*, 15512.

[50] Y. Zhang, C. Wang, G. Liu, A. Liang, L. Zhao, J. Huang, Q. Gao, B. Shen, J. Liu, C. Hu, W. Zhao, G. Chen, X. Jia, L. Yu, L. Zhao, S. He, F. Zhang, S. Zhang, F. Yang, Z. Wang, Q. Peng, Z. Xu, C. Chen, X. Zhou, *Sci. Bull.* **2017**, *62*, 950.

[51] G. Liu, H. Liu, J. Zhou, X. Wan, *J. Appl. Phys.* **2017**, *121*, 045104.

[52] Y. Sun, S. -C. Wu, B. Yan, *Phys. Rev. B* **2015**, *92*, 115428.

1700209 (8 of 8)